COMPUTATIONAL MECHANICS
New Trends and Applications
S. Idelsohn, E. Oñate and E. Dvorkin (Eds.)

NUMERICAL SIMULATION OF TURBULENT ENVIRONMENTAL FLOWS IN CLOSED WATER BODIES USING THE k-ε MODEL

Paulo C.S. Jucá, * and Clóvis R. Maliska†

* Departamento de Engenharia Mecânica(EMC)
Universidade Federal de Santa Catarina
CEP 88040-900 Florianópolis, Santa Catarina , Brazil
e-mail: emc1pcj@sinmec.ufsc.br

† Departamento de Engenharia Mecânica(EMC)
Universidade Federal de Santa Catarina
CEP 88040-900 Florianópolis, Santa Catarina, Brazil
e-mail: maliska@sinmec.ufsc.br

Key words: channel flows, turbulence, pollutant dispersion.

Abstract. *This paper describes a finite-volume method for the numerical solution of turbulent fluid flows in closed water bodies. The knowledge of the hydrodynamics of these sites is of utmost importance for determining the capacity of the water body in assimilating and dispersing any pollutant. The shear stress, acting in the surface due the wind motion causes a turbulent movement responsible for dispersing the contaminants. Since mass and momentum conservation and turbulent quantities forms a coupled set of six non-linear partial differential equations, it is required numerical techniques for solving the hydrodynamics in closed water bodies. The method uses boundary-fitted coordinates to deal with variable topography of the water body. The k-ε model is used for solving the equations for turbulent kinetic energy and its dissipation. The pressure-velocity coupling for incompressible flows is handled using the SIMPLEC method, and a colocated arrangement of the variables in the computational grid is used. The model is evaluated by solving wind driven flows and comparing the results against available experimental data. The flows are numerically solved employing different methods to impose the boundary conditions and the results show that the numerical method developed predicts well turbulent flows in closed water bodies driven by wind currents.*

1 INTRODUCTION

In studying the effects of water pollutants or sedimentation processes in closed water bodies the knowledge of it's hydrodynamic behavior is of utmost importance. This is one of the most determining factor in the capacity of the water body in assimilating and dispersing pollutants and, in a long run, an important factor in changing it's bathymetric characteristics. For a lake, for example, the hydrodynamic pattern is basically determined by the wind currents acting over its surface. The surface of a lake in a wind day shows surface waves that move toward the wind direction and transport a large amount of energy. However, this waves causes a very little transport of mass due to the oscillatory motion, since particles in waves actually moves in orbits. So, when bulk mass transport must be considered, the wave motion is not of fundamental importance. The shear stress, in the other hand, acting in the surface due the wind motion causes a turbulent movement that is not of oscillatory nature and is quite steady, the so called wind driven currents. Therefore, numerical models able to predict the flow pattern in closed water bodies such channels, lakes and lagoons are very useful tools for environmental studies. In this work it is reported the simulation of turbulent wind driven flows in closed water bodies.

To understand the circulation and pollutant transport in water bodies and also in coastal waters several numerical techniques and models have been developed in the last two decades. Most recently 3D numerical models have been implemented with different degrees of complexity in order to simulate more accurately the physical phenomena involved in this kind of problem, as can be seen in Fisher[1], Jin[2] and Huang and Spaulding[3], among others.

In the scope of the present research project Maliska et all[4] proposed a 2D model for surface discharge using boundary-fitted grids. Following, Jucá et all[5], reported a 3D model also using generalized coordinates. Recently, Jucá and Maliska[6] presented a complete 3D model for thermal and pollutant dispersion. The later one have been tested against analytical solutions[7] and experimental works[8], under laminar and turbulent flows conditions, showing very good results.

The present work reports the last improvements in the numerical model, where the k-ε turbulence model incorporated to the original model is tested under different boundary conditions.

2 THE MATHEMATICAL MODEL

Closed water bodies (or rivers) usually have irregular shapes. Therefore, the most suited coordinate system to describe their geometry is a self-conforming one, that can be adjusted to the real water body boundaries, allowing a better description of the domain. If an structured grid is used to discretize the domain, as in this work, the governing equations are more easily managed using a coordinate transformation. Using ϕ to represent any of the dependent variables in the problem, a general conservation equation can be written as

$$\frac{1}{J}\frac{\partial(\rho\phi)}{\partial t} + \frac{\partial}{\partial\xi}(\rho U\phi) + \frac{\partial}{\partial\eta}(\rho V\phi) + \frac{\partial}{\partial\gamma}(\rho W\phi) = -\hat{P}^{\phi} + \hat{S}^{\phi}$$
$$+ \frac{\partial}{\partial\xi}\left[\left(\alpha_{11} J\Gamma\frac{\partial\phi}{\partial\xi}\right) + \left(\alpha_{12} J\Gamma\frac{\partial\phi}{\partial\eta}\right) + \left(\alpha_{13} J\Gamma\frac{\partial\phi}{\partial\gamma}\right)\right]$$
$$+ \frac{\partial}{\partial\eta}\left[\left(\alpha_{21} J\Gamma\frac{\partial\phi}{\partial\xi}\right) + \left(\alpha_{22} J\Gamma\frac{\partial\phi}{\partial\eta}\right) + \left(\alpha_{23} J\Gamma\frac{\partial\phi}{\partial\gamma}\right)\right]$$
$$+ \frac{\partial}{\partial\gamma}\left[\left(\alpha_{31} J\Gamma\frac{\partial\phi}{\partial\xi}\right) + \left(\alpha_{32} J\Gamma\frac{\partial\phi}{\partial\eta}\right) + \left(\alpha_{33} J\Gamma\frac{\partial\phi}{\partial\gamma}\right)\right] \quad (1)$$

where U,V,W are the contravariant components of the velocity given by:

$$U = (u_1\xi_x + u_2\xi_y + u_3\xi_z)\ J^{-1}$$
$$V = (u_1\eta_x + u_2\eta_y + u_3\eta_z)\ J^{-1} \quad (2)$$
$$W = (u_1\gamma_x + u_2\gamma_y + u_3\gamma_z)\ J^{-1}$$

and the α_{ij} are the components of the metric tensor and J the jacobian of the coordinate transformation. As stated, ϕ represents the dependent variables for each equation. For $\phi = 1$, u_1, u_2, u_3, the mass conservation equation, momentum in x, y and z Cartesian coordinates directions are recovered, respectively. Γ represents the diffusivity transport coefficient, being zero for the mass conservation equation and equal to the effective viscosity for the Navier-Stokes equations. Also in Eq. (2) u_i represents the mean of fluctuating Cartesian velocities as defined by Rodi[9]. Details of the coordinate transformation can be found in Maliska[10].

The P^{ϕ} term is zero for the mass conservation equation. For the Navier-Stokes equations it is the pressure term given by

$$\hat{P}^{u_i} = \left[\frac{\partial p}{\partial\xi}\bar{\xi}_i + \frac{\partial p}{\partial\eta}\bar{\eta}_i + \frac{\partial p}{\partial\gamma}\bar{\gamma}_i\right] \quad (3)$$

where the subscript indicates partial derivative in the "i-th" Cartesian direction. The source term S^{ϕ} is zero for the mass conservation equation and for the Navier-Stokes equations it is written as

$$\hat{S}^{u_i} = \frac{\partial}{\partial\xi}\left[\left(J\mu_{ef}\frac{\partial U}{\partial\xi}\right)\bar{\xi}_i + \left(J\mu_{ef}\frac{\partial U}{\partial\eta}\right)\bar{\eta}_i + \left(J\mu_{ef}\frac{\partial U}{\partial\gamma}\right)\bar{\gamma}_i\right]$$
$$+ \frac{\partial}{\partial\eta}\left[\left(J\mu_{ef}\frac{\partial V}{\partial\xi}\right)\bar{\xi}_i + \left(J\mu_{ef}\frac{\partial V}{\partial\eta}\right)\bar{\eta}_i + \left(J\mu_{ef}\frac{\partial V}{\partial\gamma}\right)\bar{\gamma}_i\right]$$
$$+ \frac{\partial}{\partial\gamma}\left[\left(J\mu_{ef}\frac{\partial W}{\partial\xi}\right)\bar{\xi}_i + \left(J\mu_{ef}\frac{\partial W}{\partial\eta}\right)\bar{\eta}_i + \left(J\mu_{ef}\frac{\partial W}{\partial\gamma}\right)\bar{\gamma}_i\right] \quad (4)$$

Eq. (1), representing the system of partial differential equations governing the channel flow, is integrated in time and in a 3D elemental control volume. The pressure-velocity coupling is handled using the SIMPLEC method of Van Doormaal and Raithby[11] . Fictitious control volumes are used for the application of the boundary conditions. The resulting linear system of equations are of the form:

$$\begin{aligned} A_p \phi_p = {} & A_e \phi_E + A_w \phi_W + A_n \phi_N \\ & + A_s \phi_S + A_d \phi_D + A_f \phi_F \\ & + A_{ne} \phi_{NE} + A_{se} \phi_{SE} + A_{nw} \phi_{NW} \\ & + A_{sw} \phi_{SW} + A_{de} \phi_{DE} + A_{fe} \phi_{FE} \\ & + A_{dw} \phi_{DW} + A_{fw} \phi_{FW} + A_{dn} \phi_{DN} \\ & + A_{ds} \phi_{DS} + A_{fn} \phi_{FN} + A_{fs} \phi_{FS} + b_p \end{aligned} \tag{5}$$

for $\phi = 1, u_1, u_2, u_3$.

An equation for pressure is derived from the mass conservation equation using the SIMPLEC method. Due to the 3D nature of the problem, numerical details and expressions of the coefficients are not given. These can be found in Marchi[12] and Maliska[10]. To deal with turbulent flows a k-ε turbulence model was implemented. Thus, in Eq. (1) the effective viscosity are defined by $\mu_{ef} = \mu_t + \mu_l$, where μ_{ef} , μ_t , and μ_l are the effective, turbulent and laminar viscosity, respectively. The turbulent viscosity is given by

$$\mu_t = \rho C_\mu \frac{\kappa^2}{\varepsilon} \tag{6}$$

where $C_\mu = 0.09$, ρ is the density of the water and k and ε are the turbulent kinetic energy and its turbulent dissipation, respectively. The transport equations for k and ε also can be obtained from Eq. (1). For this, ϕ is made equal to k and ε. For k and ε the $\hat{P}^\phi$ terms are given by

$$\hat{P}^\kappa = \hat{P}^\varepsilon = 0 \tag{7}$$

and the source terms $\hat{S}^\phi$ are

$$\hat{S}^\kappa = \rho \hat{P}_{dt} - \rho\varepsilon \quad ; \quad \hat{S}^\varepsilon = \rho(C_{1\varepsilon} \frac{\varepsilon}{\kappa} \hat{P}_{dt} - C_{2\varepsilon} \frac{\varepsilon^2}{\kappa}) \tag{8}$$

The values for the constants are taken the usual ones recommended in the literature, $C_{1\varepsilon} = 1{,}44$ and $C_{2\varepsilon} = 1{,}92$. These are current values used in this kind of flows as reported in Rodi[9] and Huang and Spaulding[3]. The production term $\hat{P}_{dt}$ in the transformed space is written as

$$\hat{P}_{dt} = J\mu_{ef}\{2\left[\left(\frac{\partial u}{\partial \xi}\right)\bar{\xi}_x + \left(\frac{\partial u}{\partial \eta}\right)\bar{\eta}_x + \left(\frac{\partial u}{\partial \gamma}\right)\bar{\gamma}_x\right]^2 + 2\left[\left(\frac{\partial v}{\partial \xi}\right)\bar{\xi}_y + \left(\frac{\partial v}{\partial \eta}\right)\bar{\eta}_y + \left(\frac{\partial v}{\partial \gamma}\right)\bar{\gamma}_y\right]^2 + 2\left[\left(\frac{\partial w}{\partial \xi}\right)\bar{\xi}_z + \left(\frac{\partial w}{\partial \eta}\right)\bar{\eta}_z + \left(\frac{\partial w}{\partial \gamma}\right)\bar{\gamma}_z\right]^2 + \left[\frac{\partial}{\partial \xi}(u\bar{\xi}_y + v\bar{\xi}_x) + \frac{\partial}{\partial \eta}(u\bar{\eta}_y + v\bar{\eta}_x) + \frac{\partial}{\partial \gamma}(u\bar{\gamma}_y + v\bar{\gamma}_x)\right]^2 + \left[\frac{\partial}{\partial \xi}(u\bar{\xi}_z + w\bar{\xi}_x) + \frac{\partial}{\partial \eta}(u\bar{\eta}_z + w\bar{\eta}_x) + \frac{\partial}{\partial \gamma}(u\bar{\gamma}_z + w\bar{\gamma}_x)\right]^2 + \left[\frac{\partial}{\partial \xi}(v\bar{\xi}_z + w\bar{\xi}_y) + \frac{\partial}{\partial \eta}(v\bar{\eta}_z + w\bar{\eta}_y) + \frac{\partial}{\partial \gamma}(v\bar{\gamma}_z + w\bar{\gamma}_y)\right]^2\} \tag{9}$$

The diffusivity transport coefficient Γ for the k-ε turbulence model, see Eq (1), are given by

$$\Gamma^{\kappa} = \frac{\mu_t}{\sigma_k} \quad ; \quad \Gamma^{\varepsilon} = \frac{\mu_t}{\sigma_\varepsilon} \tag{10}$$

where the constants have the values of $\sigma_e = 1.30$ e $\sigma_k = 1.0$

3 BOUDARY CONDITIONS

In an environmental flow we have typically solid boundaries represented by the shoreline and by the bottom of the water body. At the surface the wind acts over its surface imposing a shear stress, the main driving force in determining the flow pattern in the water body. For the solid and surface boundaries no normal flux of momentum is allowed. The turbulent stresses at the solid boundaries, σ_b, are determined by

$$\sigma_b = \frac{k_v v_b}{\ln\left(\frac{\Delta Z_b}{Z_0}\right)} \tag{11}$$

where v_b is the component of the velocity *parallel to the boundary*, $k_v = 0.41$ is the Von Karman constant, ΔZ_b the distance from the boundary to the nearest grid point and Z_0 a parameter dependent on the local boundary roughness[2], assuming hydraulically smooth flow. Eq. (11), indeed, assumes that the velocity near the solid boundaries matches the logarithmic law of the wall, and for that, sufficient mesh resolution must be provided near the boundary. At the surface, the wind stress is

often calculated by[3]

$$\sigma_w = \rho_w C_d v_{wind}^2 \tag{12}$$

where C_d is the air-water drag coefficient, ρ_w the air density and v_{wind} it's velocity, measured at 10 m. height. In the present work, the stresses due to wind are know from experimental data.

The stresses at the top and bottom boundary can be used for applying boundary conditions for the velocity. As a simple example, if the plane xy is parallel to the surface and bottom, and z is along the depth, the bottom stress can be approximated by

$$\sigma_{ib} = \mu_{ef}\left(\frac{u_{ib} - u_{ip}}{2Z_b}\right) \tag{13}$$

where "i" represents the "i-th" Cartesian direction (i = 1,2).

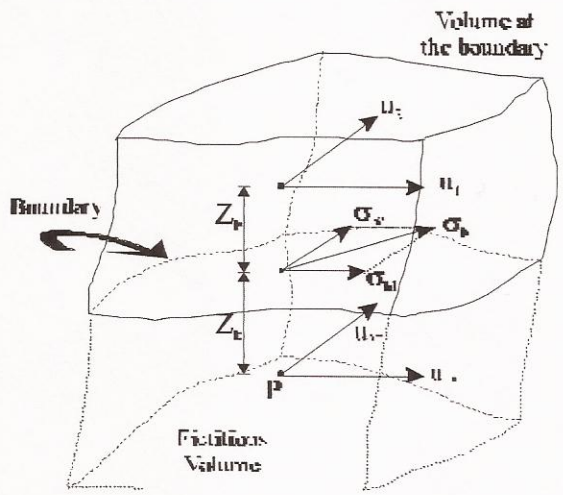

Figure 1 - Turbulent tension sketch at the boundary

Rewriting

$$u_{ip} = u_{ib} - \left(\frac{2Z_b \sigma_{ib}}{\mu_{ef}}\right) \tag{14}$$

which imposes the boundary conditions for the velocity. The turbulent kinetic energy and its dissipation at solid boundaries are determined following Rodi [9], as

$$\kappa_b = \frac{v_*^2}{(C_\mu)^{0.5}}; \qquad \varepsilon_b = \frac{v_*^3}{k\Delta Z} \tag{15}$$

At the bottom, the resulting shear velocity is

$$v_* = \sqrt{\frac{(\sigma_{1b}^2 + \sigma_{2b}^2)^{0.5}}{\rho}} \tag{16}$$

where v_* is the friction velocity. Using the surface stress, the k and ε values at the surface can be calculated using Eq. (15)

Equations (11) to (16) shows the usual way boundary conditions can be imposed when the friction velocity at the surface is know from (12) and the log wall rule is employed at the bottom. The main goal is allow a consistent estimate for the values of k and ε at both boundaries, Eq. (15). This kind of boundary condition were used with success in this model as reported in Jucá and Maliska [7]

An alternative way is also employed in this work in order to test the mathematical model capabilities and confidence. Suppose the velocities at the surface and bottom are imposed, being their values known by experimental measurements. These velocities are then used as boundary conditions for the Navier-Stokes equations, and the stresses needed to evaluate the k and ε boundary conditions, through Eq. (15), can be taken, at the surface, from the derivative of the velocity profile near this boundaries in each time step. At the bottom boundary the stresses can be also taken from the velocity profile (VP condition) or, as an alternative way, from the log wall rule (LWR condition), Eq(11).

4 MODEL VERIFICATION

In order to test the proposed model, the experiments carried out by Baynes-Knapp [13] and Tsanis [14,15] were selected. These were choose since they were performed in different experimental devices and also reports data enough to impose the two kinds of boundary conditions former described .

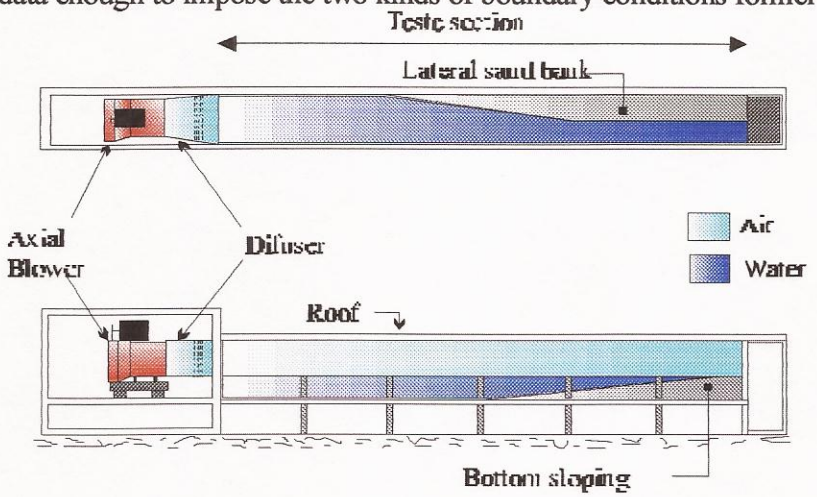

Figure 2 - Typical air -water test channel, Baines-Knapp[13]

Baynes-Knapp experiments were carried out in an air-water tunnel shown in Figure 2. The channel was 42 ft long and have a 3 x 3 ft cross-section. Most of the channel was covered, and a 3 hp axial blower were responsible for the air currents generated during the experiments. Measurements were taken for mean intake air velocities of 3,84 m/s and 6,0 m/s. For each one the velocity profiles and pressure drop along the tunnel were measured. For further information about the experiment device and measuring techniques refer to Baines-Knapp [13].

The experiments performed by Tsanis were made in a conceptually different device, as show in Figure 3.

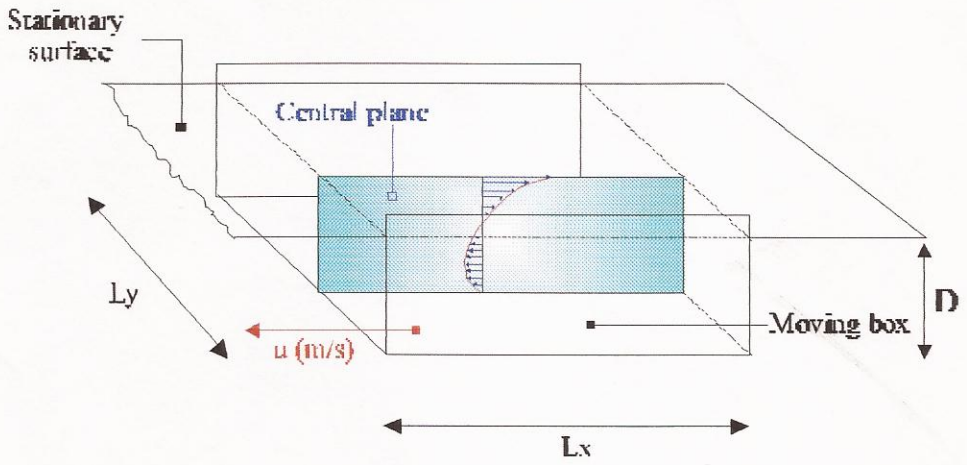

Figure 3 - Experimental method used by Tsanis [14,15]

In this device the water body is represented by the air volume inside the box. This box (with no top), move along a stationary surface, which represents the air water interface. During the experiments the box (Lx = 2,4 m ; Ly = 0,95m) move at a maximum speed of 3 m/s, and have lateral walls made of pexiglass in order to permit the flow visualization and measurements. The stationary surface were 31 m. long. For further information on the experimental device and measuring techniques refer to Tsanis [14,15].

The Baines-Knapp experiments are resumed in Table 1, were the surface velocities and stresses are reported, for two Reynolds numbers, defined by

$$Rs = \frac{\rho u_s D}{\mu} \tag{16}$$

As those experiments were performed for typical two dimensional channel flows, the boundary conditions for the 3D model, in order to adapt the model to this kind of flow, are show in the Figure 4. To recover the 2D flow, symmetry boundary conditions were used for the north and south faces.

Table1 - Data and experimental results,Baines e Knapp [13]

Description	Symbol	Unit	Experiment 1	Experiment 2
Height	D	m	0,3048	0,3048
Wind Velocity	u_a	m/s	3,901	6,096
Surface friction velocity	u_{*s}	cm/s	0,6233	0,9416
Surface velocity	u_s	cm/s	10,72	15,25
Reynolds number	R_s	#	32700	46500
Normalized surface velocity	u_s/u_{*s}	#	17,2	16,2
Equivalent roughness height	z_{ob}	mm	0,3521	0,4795
Zero velocity height	z_{v0}/D	#	0,69	0,68

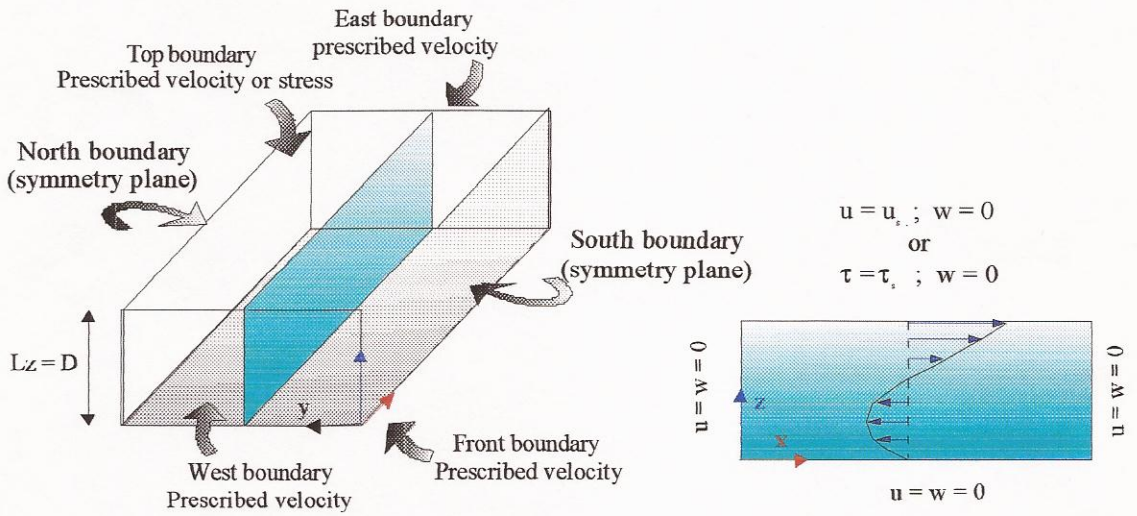

Figure 4 - 2D flow in a closed channel: boundary conditions.

4 RESULTS

Tsanis [14,15] reports velocity profiles in the test section of the channel for low Reynolds numbers, 3000, 5000 and 8000, as defined by Eq(16). Using the log wall rule at the bottom boundary to estimate the stresses (LWR condition) and also the k and ε values, Figure 5 compares the velocity profiles predicted by the numerical model against the experimental results. For these experiments, in

Eq. (11), the value of $Z_0 = 1.4 \times 10^{-4} * D$ was used, as sugested by Tsanis.

As shown, the numerical velocity profiles are in a good agreement with the experimental data, although the low Reynolds can not assure a completely turbulent flow, as stated by Tsanis.

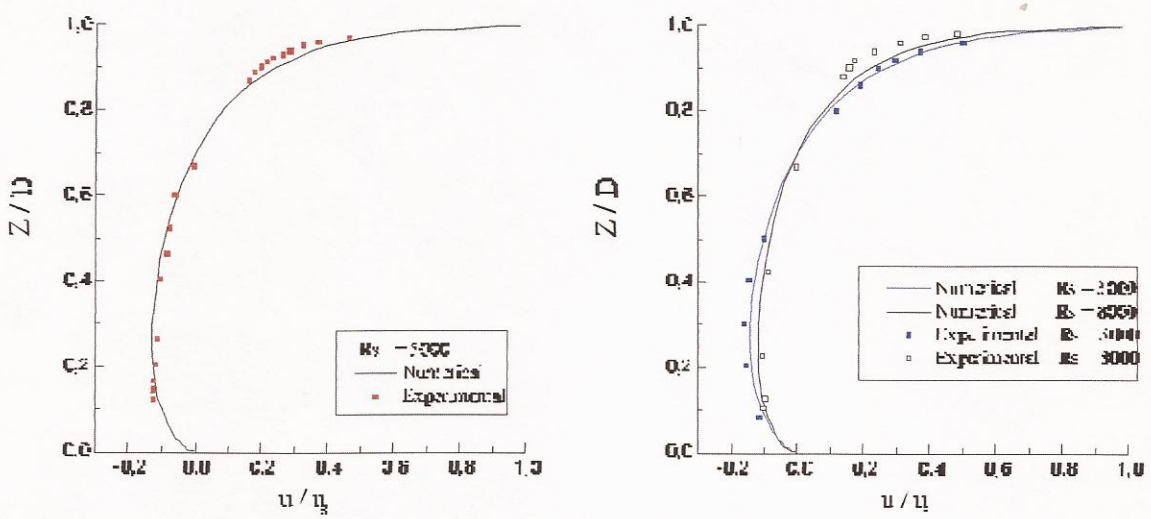

Figure 5 - Velocity profiles employing the log wall rule at bottom

The same numerical experiments was performed, considering now the velocity for estimating the bottom stress (VP condition). The results obtained are shown in the Figures from 6 to 8. Each of these pictures also depicts the effective viscosity profile (μ_{ef}) obtained by the k-ε model. The effective viscosity profile proposed by Tsanis[14] for this kind of flow is also provided in each figure. This viscosity profile is defined by

$$\nu = \frac{\mu}{\rho} = \left(\frac{\lambda u_{*_s}}{D}\right)\left(z + z_b\right)\left(D - z + z_s\right) \tag{17}$$

where $u_{*_s} = \sqrt{\frac{\tau_s}{\rho}}$ is the surface friction velocity and λ a constant that resembles the intensity of the turbulence. Its recommended value is $\lambda = 0.35$, although it can varies accordingly the Reynolds number as follows

$$10^3 \leq \quad Rs = \frac{\rho u_s D}{\mu} \quad \leq 10^5 \qquad 0{,}20 \quad \leq \quad \lambda \quad \leq \quad 0{,}50$$

The constants z_b e z_s are the characteristic lengt at the bottom and surface, respectively, which represent the relative measure of the laminar sub layer in the flow. Tsanis recommends the values for z_s and z_b

$$z_s = 2{,}20 \times 10^{-4}\, D \quad \text{and} \quad z_b = 0{,}60 \times 10^{-4}\, D$$

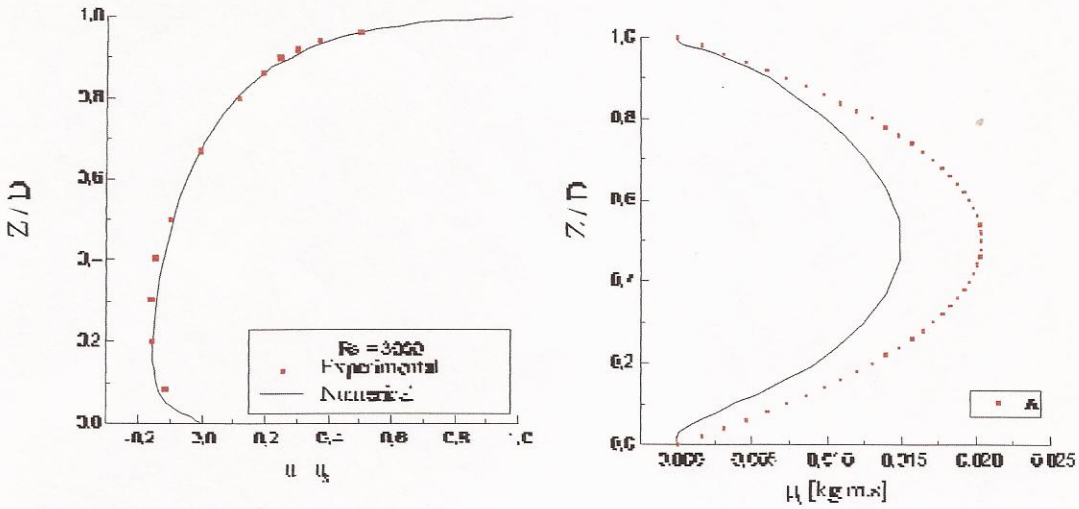

Figure 6 - Numerical results for the velocity profile(A: μprofile for $u_{*_s} = 0{,}7657\ 10^{1}$ cm/s, Eq.(17))

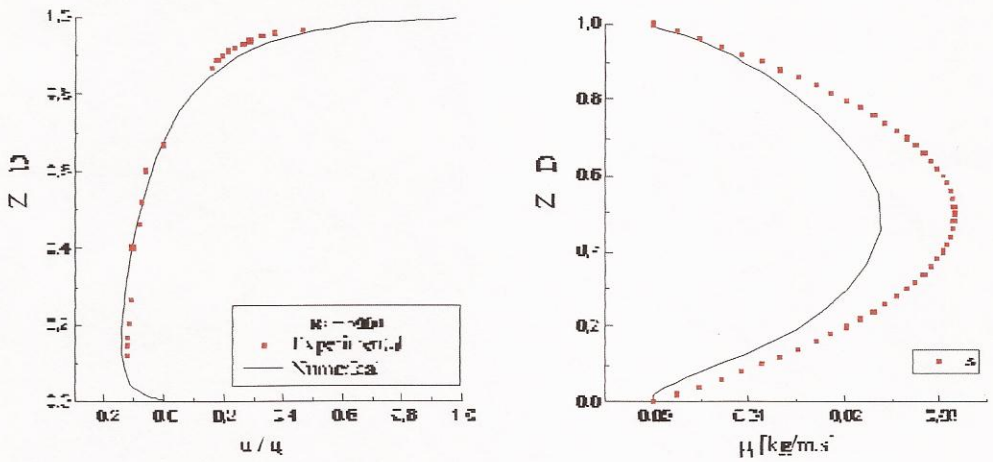

Figure 7 - Numerical results for the velocity profile(A:μ profile for $u_{*_s} = 0{,}1185$ cm/s, Eq.(17))

As in the preceding cases, the velocity profiles are in good agreement with the experimental data, nevertheless a different approach for applying boundary condition was employed.

The viscosity profiles obtained from Eq.(17) use the surface shear stress calculated from the velocity profile. Also the constants in the Eq.(17) were taken as indicated and no adjustments were made in these values, in order to obtain a better agreement between the profiles.

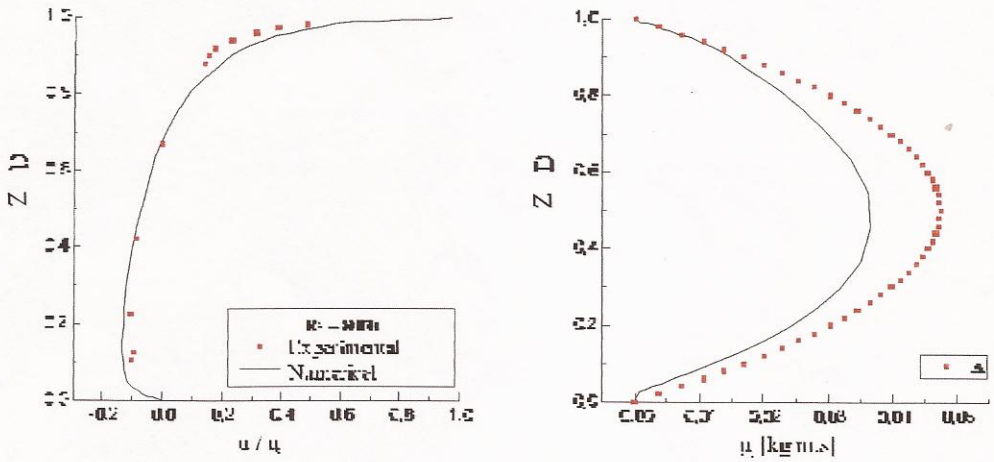

Figure 8 - Numerical results for the velocity profile(A:μ profile for u_{*_s} = 0,1783 cm/s, Eq.(17))

The Tsanis experiments denoted the capability of the numerical model for low Reynolds number flows. The Baines-Knapp's experiments can now be used to verify the performance at higher Reynolds numbers.

As Baines-Knapp reports the friction velocity and the velocity at the surface, in this case we opt by imposing velocity boundary conditions (VP condition) at bottom and surface, and, from the velocity profile estimate the stresses at these boundaries and so the k and ε for these boundaries. These also allows the comparison between the stresses measured in the experiment against the one provided by the numerical model. These are also indicated in each figure.

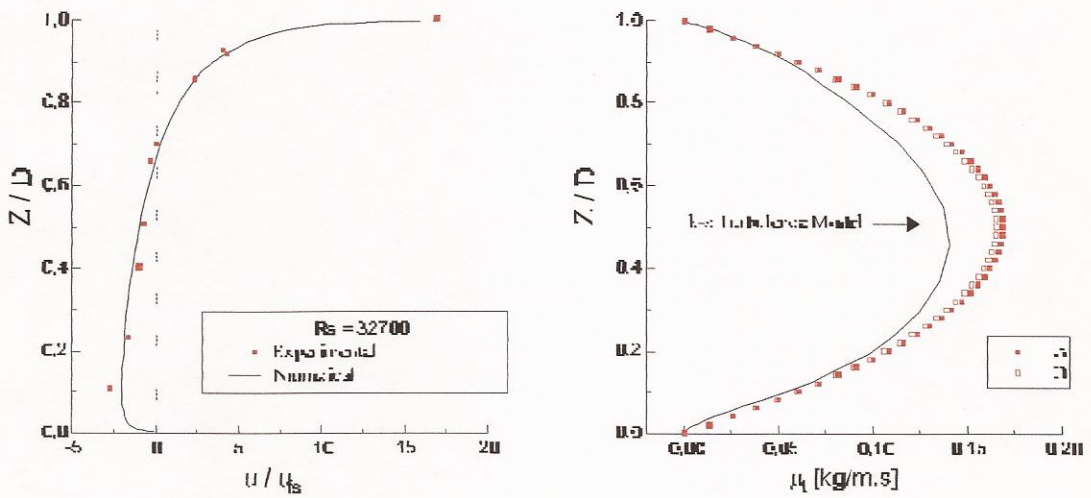

Figure 9 - Velocity profiles for Rs = 32700.(A; μprofile for the numerical estimated u_{*_s} = 0,636 cm/s; Bμ profile for experimental u_{*_s} = 0,6233 cm/s; A and B from Eq(17))

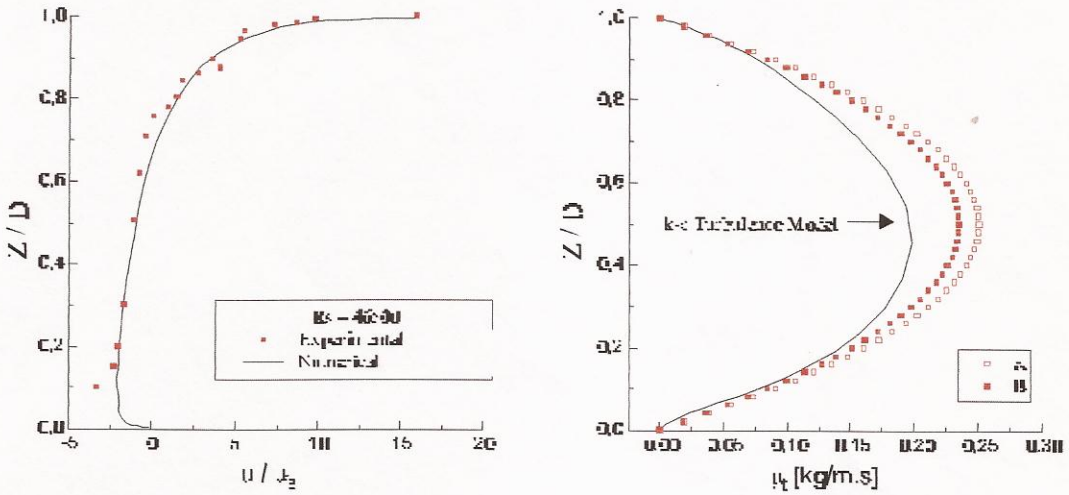

Figure 10 - Velocity profiles for Rs = 46500.(Aμ profile for the numerical estimated u_{*s} = 0,8835 cm/s; Bμ profile for experimental u_{*s} = 0,9416 cm/s; A and B from Eq(17))

Again the agreement between the numerical and experimental results are good, except for the region near the bottom. But, as pointed out by Baines and Knapp, the velocity peak that occurs in the experimental velocity profile is due to the presence of a sloping sand bank at the end of the channel and also to its short length. Also only few measurement points were available near the bottom.

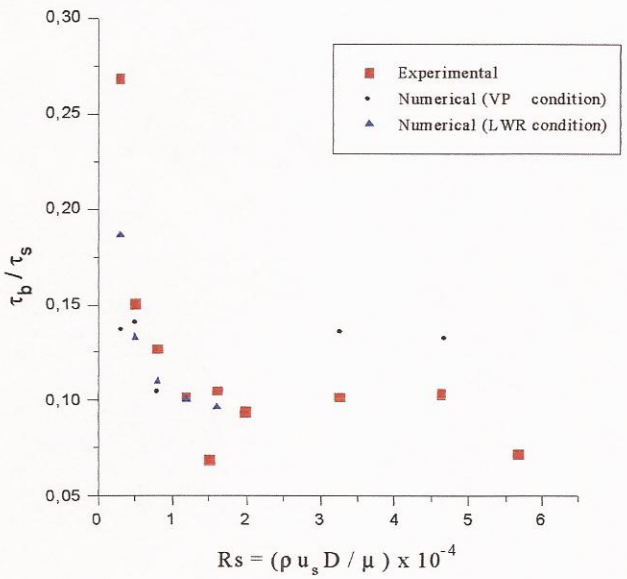

Figure 11 - Relation σ_b / σ_s

By the velocity profiles obtained before, we can estimate the stresses at the bottom and at the surface. The relation between these stresses, although do not follow a clear tendency as show in Figure 10, can testify the confidence of the numerical model using both kinds of boundary conditions. As we can see the same tendency provided by the experimental data is verified in the numerical results. The experimental data was assembled by Tsanis[15] from his experiments and from others.

5 CONCLUSIONS

This work reports numerical results using a boundary-fitted, co-located finite-volume method for the solution of turbulent fluid flows in closed water bodies. The main goal is the prediction of three-dimensional dispersion of pollutants in water bodies.

Several comparisons were made against experimental results demonstrating the ability of the model in well predicting the turbulent fluid flow. The surface and bottom shear stresses also show the correct trend shown by the experimental results. For the class of 2D flows resolved, the turbulent viscosity obtained with the k-ε method agree well with that proposed by Tsanis.

Two different methods for applying boundary conditions at the bottom boundary were used, both demonstrating good agreements with the experimental results. The next step is to add to the equation system the mass conservation equation for pollutants, allowing the prediction of pollutant dispersion in water bodies.

REFERENCES

[1] H.B. Fisher, *Transport Models for Inland and Coastal Waters*, New York, Academic Press, 542 pp., Proceedings of a Symposium on Predictive Ability (1981)

[2] X.Y. Jin, *Quasi-Tridimensional Numerical Modeling of Flow and Dispersion in Shallow Water*, Communication on Hydraulic and Geotechnical Engineering, Dp of Civil Eng., Delft Univ. of Technology, Rep. 93-03, ISSN 0169-6548 (1993)

[3] W. Huang, M. Spaulding, *3D Model of Estuarine Circulation and Water Quality Induced by Surface Discharges*, Journal of Hydraulic Eng., vol. 121, No 4, pp. 300-311 (1995)

[4] C.R. Maliska, A.F.C. Silva, S. Polina, J.A.O. Perez, , *Heat Transfer Predictions of Thermal Discharges in Water Bodies*, IX Congresso Brasileiro de Engenharia Mecânica, pp. 45-48, Florianópolis, SC, Brazil (1987)

[5] P.C.S. Jucá, A.F.C. Silva, C.R. Maliska, *Solução Numérica de Problemas Tridimensionais Elípticos de Convecção de Calor*, X Congresso Brasileiro de Engenharia Mecânica, pp. 161-164, Rio de Janeiro, Brazil1(1989)

[6] P.C.S. Jucá, C.R. Maliska, *Tridimensional Simulation of Pollutant Dispersion in Water Bodies*, XVI Congresso Íbero Latino - Americano sobre Métodos Computacionais para Engenharia, vol. 1, pp. 640-649, Curitiba, Brazil (1995)

[7] P.C.S. Jucá, and C.R. Maliska, *Turbulent Water Channel Flows Under Surface Wind Action*, Proceedings of the 6th Brazilian Congress of Engeneering and Thermal Sciences - ENCIT and Latin American Congress of Heat and Mass Transfer - LATCYN, vol I, pp 383-338, Florianópolis, SC, Brasil (1996)

[8] P.C.S. Jucá, and C.R. Maliska, *Numerical Simulation of Turbulent Environmental Flows*, Anais XVIII CILANCE - Congresso Íbero Latino - Americano de Métodos Computacionais para Engenharia, vol 1, pp 203-210,Brasília, DF, Brasil, Outubro (1997)

[9] W. Rodi, *Turbulence Models and Their Application in Hydraulics*, Int. Assoc. for Hydraulic Research , Delft, Netherlands (1980).

[10] C.R. Maliska, *Transferência de Calor e Mecânica dos Fluidos Computacional: Fundamentos e Coordenadas Generalizadas*, Livros Técnicos e Científicos Editora (1995)

[11] J.P.Van Doormaal, G.D. Raithby, *Enhancements of the SIMPLE Method for Predicting Incompressible Fluid Flow*, Num. Heat Transfer, vol. 7 pp. 147-163 (1984)

[12] C.H. Marchi, "Solução Numérica de Escoamentos Tridimensionais Viscosos em Qualquer Regime de Velocidade", Dissertação de Mestrado, Curso de Pós-Graduação em Engenharia Mecânica, Departamento de Engenharia Mecânica, Centro Tecnológico, Universidade Federal de Santa Catarina (1992)

[13] W.D. Baines, D. Knapp , *Wind Driven Water Currents*, Hydraulic Division, Proceedings of the American Society of Civil Engineers, vol. 91, March, pp. 205-221(1965)

[14] I.K. Tsanis, *Simulation of Wind-Induced Water Currents*, Journal of Hydraulic Engeneering, vol. 115, No. 8, August, pp 1113-1134 (1989)

[15] I.K. Tsanis, *The Structure of Turbulent Shear-induced countercurrent Flow*, Journal of Fluid Mechanics, vol. 189, pp. 531-552 (1988)